

# Constrained hyperelastic parameters reconstruction of PVA (Polyvinyl Alcohol) phantom undergoing large deformation

Hatef Mehrabian<sup>\*a</sup>, Abbas Samani<sup>a,b,c</sup>

<sup>a</sup>Department of Electrical & Computer Engineering, University of Western Ontario, London, ON, Canada

<sup>b</sup>Department of Medical Biophysics, University of Western Ontario, London, ON, Canada

<sup>c</sup>Imaging Research Laboratories, Robarts Research Institute, London, ON, Canada

## ABSTRACT

The nonlinear mechanical behavior of tissues that undergo large deformations, e.g. the breast, is characterized by hyperelastic parameters. These parameters take into account both types of nonlinearities: tissue intrinsic nonlinearity and geometric nonlinearity. Elastography technique capable of tissue hyperelastic parameter reconstruction has important clinical applications such as cancer diagnosis and interventional procedure planning. In this study we report our progress on the development of constrained reconstruction technique of breast tissue hyperelastic parameters [1]. The extension of this work is twofold: the inclusion of the popular Veronda-Westmann hyperelastic model and using a novel technique for tissue displacement tracking. This tracking technique is based on the Horn-Schunck optical flow method [2]. The objective of this paper is to validate the numerical analysis performed in [1] by phantom experiment. For this purpose, a PVA (Polyvinyl Alcohol) phantom that consists of three tissue types was constructed and tested. PVA exhibits nonlinear mechanical behavior and has been recently used for tissue mimicking purposes. Reconstruction results showed that it is feasible to find the relative hyperelastic parameters of the tissue with acceptable accuracy. The error reported for the relative parameter reconstruction was less than 20%, which may be sufficient for cancer diagnosis purposes.

**Keywords:** Disease Characterization, Modeling, Hyperelasticity, Constrained Reconstruction, Polyvinyl Alcohol

## 1. INTRODUCTION

One of the most common forms of cancer in women is breast cancer. It is the second most common type of cancer [3] and is the fifth most common cause of cancer death. Statistics shows that one in 9 women is expected to develop breast cancer during her lifetime; one in 28 will die of it [4]. Thus, early detection and diagnosis of breast cancer is very important. Several techniques have been developed to accomplish this goal such as x-ray mammography, ultrasound and magnetic resonance imaging, and recently elastography. Among these methods, elastography is a novel technique that has shown promising results in breast cancer detection and diagnosis.

It has been known that changes in the mechanical behavior of soft tissues are associated with pathological processes. Various pathologies in breast tissue exhibit different nonlinear mechanical characteristics [5]. This has set the motivation for the concept of elastography using which images of the elastic properties of soft tissues can be obtained. The goal of elasticity imaging is to map mechanical properties of soft tissues such as Young's modulus, Poisson's ratio, viscosity, etc., in an anatomically meaningful way to provide useful clinical information [6]. Recently, elastography has become a subject of interest for many researchers as it has the potential to be an effective non-invasive technique for cancer detection and diagnosis.

Due to low stiffness and lack of mechanical constraints, breast tissue undergoes large deformation during elastography test. Thus, its deformation cannot be modeled using linear biomechanical models, which are valid for only a small range of strains. Furthermore, elastography images usually provide tissue elastic modulus ratio. Given the breast tissue

\*hmehrab@uwo.ca; phone 1 416 826-3273;

nonlinearity, the reconstructed ratio will be strongly dependent on the amount of pre-compression applied to the tissue during the test. Moreover, researchers demonstrated that the contrast of elastogram and the CNR (contrast to noise ratio) in elastography alter significantly as a result of change in tissue modulus [7].

In [1] we showed by numerical simulation that it is possible to reconstruct hyperelastic parameters of soft tissues using pre- and post-compression images. The objective of this study is to validate our numerical analysis by phantom experiment, and to extend the presented method for Veronda-Westmann model. Here, we developed a constrained mechanical behavior reconstruction algorithm based on the linear method presented by Samani *et al* [8]. This constrained reconstruction assumed that the geometry of the phantom before compression is known and that the loading is quasi-static. It also assumes that the tissues are homogeneous having constant mechanical properties throughout the volume of each tissue type.

In this article we first describe the reconstruction algorithm and the results of its application to the Veronda-Westmann model. Then, the hyperelastic phantom constructed for the experiment is described. Next, the uniaxial compression test results are reported. This is followed by describing the assumptions that are used in the study along with introduction of a novel displacement acquisition technique we developed based on a hierarchical Horn-Schunck optical flow method. Finally the application of the proposed reconstruction technique on the PVA phantom is demonstrated.

## 2. THEORY AND METHODS

### 2.1 Reconstruction technique

Hyperelastic parameters of soft tissues are reconstructed using the iterative approach we proposed recently [1]. This iterative approach was developed in conjunction with the Polynomial and Yeoh hyperelastic models for soft tissues. This approach is summarized in the flowchart given in Fig. 1. Here, we extended our technique to include the Veronda-Westmann hyperelastic model. Having an exponential form, the Veronda-Westmann strain energy function has been recently used by several researchers in modeling nonlinear behavior of soft tissues, particularly in modeling breast tissues [9]. This strain energy function is given in Equation (1).

$$U_{Veronda-Westmann} = C1(e^{C3(I_3-1)} - 1) + C2(I_2 - 3) \quad (1)$$

The reconstruction approach uses the governing equation of stress-deformation, which is given in Equation (2).

$$\sigma = \frac{2}{J} DEV \left[ \left( \frac{\partial U}{\partial I_1} + \overline{I_1} \frac{\partial U}{\partial I_2} \right) \overline{B} - \frac{\partial U}{\partial I_2} \overline{B} \cdot \overline{B} \right] - pI, \quad (2)$$

where  $DEV$  represents the deviatoric part of the stress tensor,  $P$  is the hydrostatic pressure and  $I$  is the identity matrix. The other parameters are defined below:

$$J = \det(F), \quad \overline{F} = J^{-1/3} F, \quad \overline{B} = \overline{F} \cdot \overline{F}^T, \quad \overline{I_1} = tr(\overline{B}), \quad \overline{I_2} = \frac{1}{2} (\overline{I_1}^2 - tr(\overline{B} \cdot \overline{B}))$$

where  $F$  is the deformation gradient tensor. Equation (2) is rearranged for the Veronda-Westmann model parameters to obtain the nonlinear system given in Equation (3).

$$\{\sigma\} = f(\{C\}) \quad (3)$$

Where  $\{\sigma\}$  is the element stress tensor,  $f(\cdot)$  is a function of nodal displacements, and  $\{C\}$  is the unknown hyperelastic parameters. This non-linear system of equations is solved using a non-linear least squares method that involves iteratively using a combination of preconditioned conjugate gradient optimization method, steepest descent method and the Newton's optimization method.

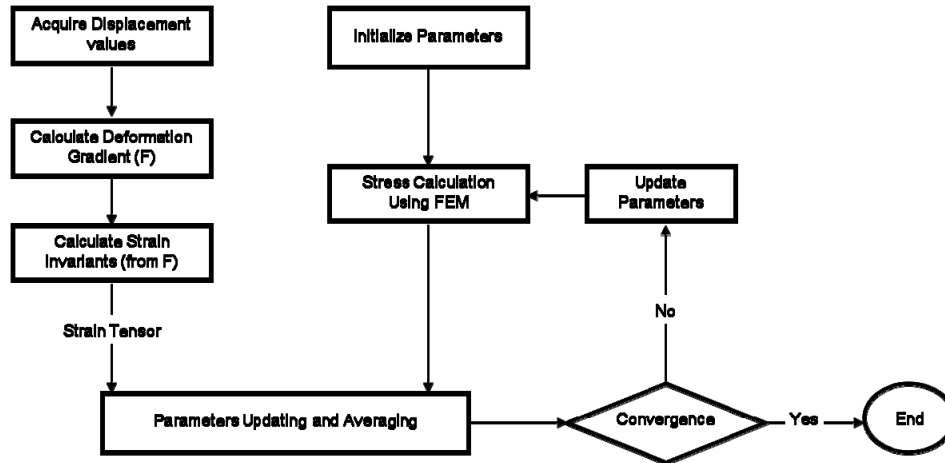


Fig. 1: Flow chart illustrating the procedure of iterative reconstruction of hyperelastic parameters

## 2.2 Numerical phantom

A numerical phantom was constructed to validate the method using Veronda-Westmann model by simulation. This phantom is identical to the one that was used in [1] for Yeoh and Polynomial models. The phantom is comprised of a cylinder connected to a hemisphere which represents a simplified breast geometry. The phantom is 3-D and is made up of 8-noded elements. It has three different tissue types, as shown in Fig. 2, to represent all three tissue types present in a cancerous breast (adipose tissue, fibroglandular tissue and tumor tissue).

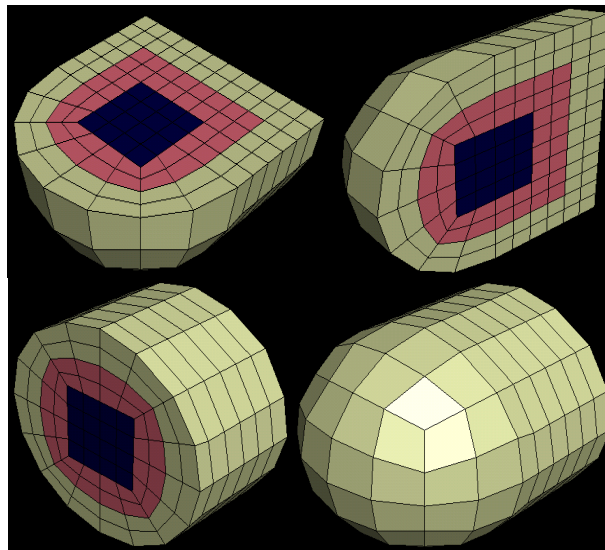


Fig. 2: FE mesh of the computational breast phantom and three corresponding orthogonal cross sections. Different tissue types are shown in different grayscale colors, where the interior, middle and exterior layers represent tumor, fibroglandular and adipose tissues, respectively.

Displacement boundary condition is applied to the top nodes of this phantom and zero displacement boundary condition is applied to its bottom nodes. The loading is quasi-static to satisfy the conditions required for constrained reconstruction. In this stage of the investigation we assume that the hyperelastic parameters for the normal breast tissues (the adipose and the fibroglandular tissues) are known, and we try to determine the parameters for the tumor tissue. Samani *et al* [10] indicated that the hyperelastic parameters of the normal breast tissues can be measured independently. They reported these parameters for a Polynomial model of normal breast tissues.

### 2.3 Experimental phantom construction

To validate the presented reconstruction algorithm experimentally, a phantom is constructed that exhibits non-linear mechanical behavior similar to that of breast tissues. Polyvinyl alcohol-cryogel (PVA-c) 99% is used to construct this phantom. PVA-c hydrogels have been studied and used previously in the biomedical field for mimicking soft tissue behavior [11,12]. High physical strength appears in PVA-c as a result of the chemical cross-linking of its hydrogels [13-15]. The degree of cross-linking of PVA hydrogels is increased by having its aqueous solution undergo freeze-thaw cycles (FTC's). Freezing and thawing of the PVA solution causes the aqueous mixture to cross-link via hydrogen bonding of the hydroxyl groups on the PVA molecules. This cross-linking is fully reversible by heating the PVA-c above 70°C.

The phantom, shown in Fig. 3 is constructed using three different tissue types with distinct mechanical behaviors to simulate breast's fat, fibroglandular and tumor tissues. To achieve this, the inner cylindrical part is made using 10% PVA (10% PVA powder solved in 90% deionized water), 0.2% biocide and 5 FTC's. This part simulates the tumor in the tissue and has the highest stiffness. The middle block shape part that surrounds the tumor is constructed from 5% PVA, 0.2% biocide and 3FTC's. Finally, the outer part of the phantom is made up of 5% PVA, 0.2% biocide and 2 FTC's.



Fig. 3: The PVA phantom, which consists of three different tissue types. Two outer and middle block shape portions represent the adipose and fibroglandular tissues of the breast while the inner cylindrical part represents a breast tumor.

These specifications are chosen in a way that the stiffness ratio of the tumor, the middle tissue and the outer tissue are 5, 2 and 1 respectively. Food coloring is added to the PVA's as contrast agent to make each tissue type separable in the photo images. This contrast agent has no impact on the mechanical behavior of the PVA.

### 2.4 Uniaxial compression test for PVA samples

Hyperelastic parameters of each tissue type are found independently by performing uniaxial compression test on cylindrical samples of the same tissue. The uniaxial test is performed using the electromechanical system developed by Samani *et al* [16]. Fig. 4 shows the setup made for uniaxial compression test. This setup is made such that it applies uniform force to the top of the sample and records this applied force using a load cell. The displacement accuracy of this system is  $2 \mu m$ . Thus, it is capable of recording the force and the amount of compression applied to the cylinder with high accuracy.

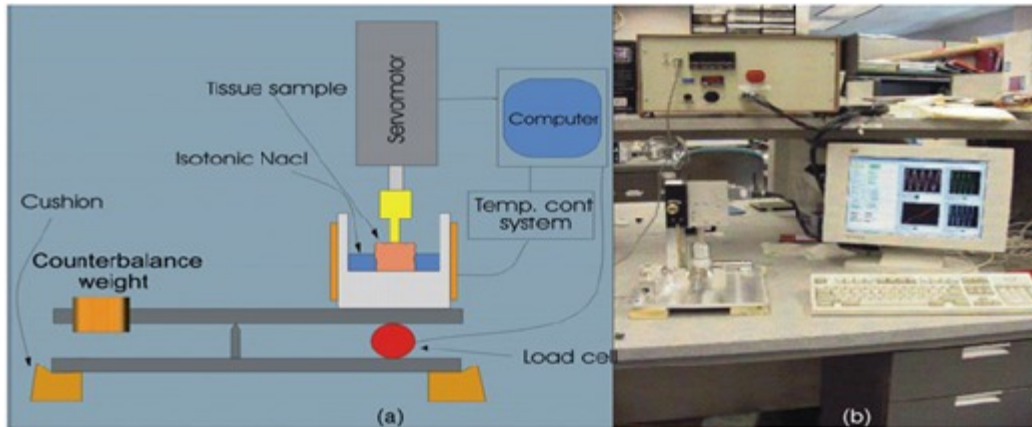


Fig. 4: a) Schematic of uniaxial compression test setup, b) photograph of the uniaxial compression setup

The PVA samples have an equal height and diameter of approximately  $1\text{ cm}$  and are shown in Fig. 5.

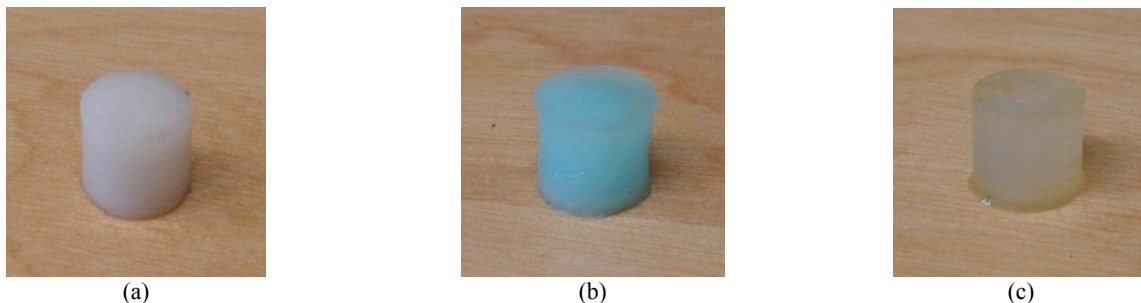


Fig. 5: a, b and c) Cylindrical samples of the tumor (inner white cylindrical part of the phantom), fibroglandular tissue (middle blue cubic part of the phantom), and the adipose (outer yellow cubic part of the phantom), respectively. These samples were made for uniaxial compression tests of the PVA phantom layers.

Using the electromechanical setup described earlier, we acquired the force-deformation data for each sample. We applied  $1\text{ g}$  preload for the measurements and used the maximum compression range of the system which is  $25\text{ mm}$ . The hyperelastic parameters of each tissue type calculated using the force-deformation curves for the Veronda-Westmann model are given in Table 1.

Table 1: The hyperelastic parameters of the white (tumor), blue (fibrogland) and yellow (adipose) cylindrical sample for Veronda-Westmann strain energy functions.

Coefficients	C1	C2	C3
White(Tumor)	0.0091	-0.0017	2.5875
Blue(Fibrogland)	0.0066	-0.003	2.0039
Yellow(Adipose)	0.0043	-0.0006	1.5564

## 2.5 Plane stress assumption

The phantom shape is made in a way that it is close to a plane stress situation. The dimensions of the phantom are  $2\text{ cm} \times 6.1\text{ cm} \times 6.3\text{ cm}$ . The thickness is small compared to its other dimensions, thus we can assume that the system performs like plane stress condition. Plane stress assumption is used here to convert the 3-D analysis to a simple 2-D plane stress analysis. 3-D analysis is time consuming since our reconstruction algorithm involves employing ABAQUS (commercial FE software) to solve a nonlinear finite element problem based on hyperelastic formulation in each iteration. For this nonlinear FE problem conducting 2-D analysis is significantly faster than 3-D analysis. Another advantage of using the plane stress assumption is simplifying the image processing step required to estimate tissue displacements. Under plane stress conditions the deformations of the nodes along the direction of thickness are identical.

Therefore, using this assumption, only the displacements of the nodes on the surface are needed and the analysis can be performed on a simplified 2-D phantom model.

To validate the accuracy of the plane stress assumption, a numerical study was performed using ABAQUS software. This study involved performing 3-D and 2-D (plane stress) analyses of a numerical phantom and comparing the results. The geometry and specifications of the phantom are the same as those of our experimental phantom. The in-plane nodal displacements of the 3-D phantom model, the nodal displacements of the plane stress model, and their differences (errors) are given in Table 2.

Table 2: Numerical phantom's mean and maximum values of displacements calculated using the 2-D plane stress and 3-D models and the corresponding errors for both X-axis and Y-axis.

	Mean value of displacement (X-axis)	Max value of displacement (X-axis)	Mean value of displacement (Y-axis)	Max value of displacement (Y-axis)
<b>2-Dimensional model</b>	0.2357 (cm)	0.4805 (cm)	0.75 (cm)	1.5(cm)
<b>3-Dimensional model</b>	0.2276 (cm)	0.4690 (cm)	0.75 (cm)	1.5(cm)
<b>Error percent b/w two models</b>	0.3615%	2.6861 %	3.5735%	5.3018%

As shown in this table, the errors are less than 5% showing that this assumption is valid. Therefore, we use this assumption for designing our experiment.

## 2.6 Displacement data acquisition

We applied 31.7% compression to the phantom. To acquire the resulting tissue displacements data, we developed a novel optical flow based technique we used here [2]. The method takes advantage of having the mechanical model of the tissue. It constructs the numerical model of the phantom by making an rough estimate of the properties of the soft tissues and follows an iterative procedure by employing a hierarchical coarse to fine Horn-Schunck optical flow method at each iteration. Unlike in conventional optical flow techniques, this hierarchical approach is capable of estimating large displacements. The Horn-Schunck method [17] combines gradient constraint with a global smoothness term to constrain the estimated velocity field  $v(x, t) = (u(x, t), v(x, t))$  by minimizing Equation (4) defined over domain  $D$ ,

$$\int_D (\nabla I \cdot v + I_t)^2 + \lambda^2 (\|\nabla u\|_2^2 + \|\nabla v\|_2^2) dx \quad (4)$$

In this method, we use as input a frame sequence of the phantom consisting of 2 images taken at different compression levels (0% and 31.7% compression levels). Starting from blurred coarse images, this hierarchical method employs the Horn-Schunck method between the two consecutive images to estimate the corresponding displacements. This is followed by deforming the baseline (0% compression) image. This iterative displacement updating followed by image deformation is continued until the numerically deformed image and the deformed image are approximately identical. The photo of the phantom before compression was taken using a digital camera. The phantom was compressed using the set up shown in Fig. 6 and the compressed image was taken using the same digital camera and from the same distance. In this experiment we applied a maximum of 31.7% compression to the phantom with zero displacement boundary condition at the bottom. The photos of the phantom at 0% and 31.7% compression levels are depicted in Fig. 6.

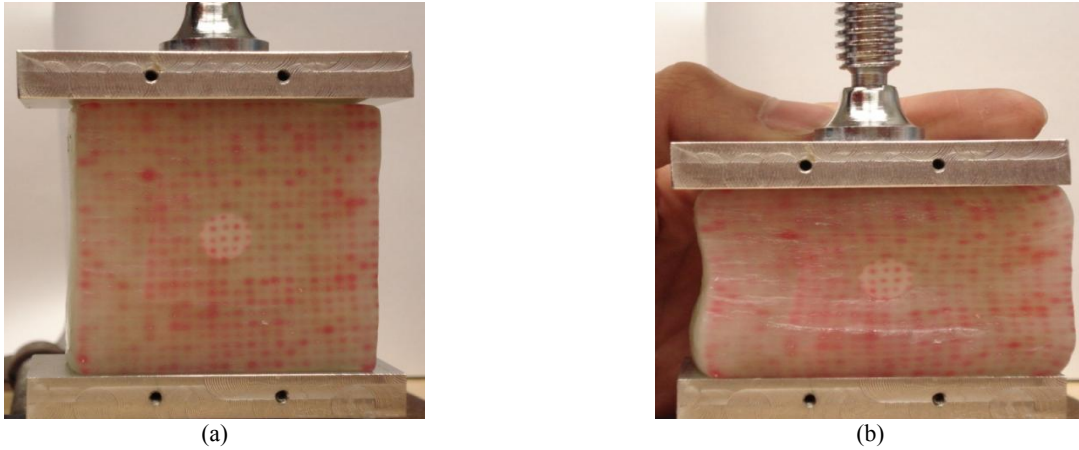


Fig. 6. a) Image of the phantom before compression and b) image of the phantom after compression

### 2.7 Hyperelastic Parameter Reconstruction

Hyperelastic parameters of the tumor tissue in the phantom are reconstructed using the iterative approach presented for the numerical analysis. The approach is presented in the flowchart given in Fig. 1. The displacement field is acquired from the optical flow processing. This displacement field is then fed to the algorithm to calculate the deformation gradient and strain invariants. The iterative procedure starts with an initial guess for the parameters. Then, ABAQUS is employed for stress calculation at each iteration. Using the governing equation for stress-deformation relationship, a new set of hyperelastic parameters is calculated. This continues until the stress calculated using the displacement data converges to the stress that is calculated by ABAQUS.

## 3. RESULTS

### 3.1 Numerical Validation

The results of the numerical phantom described in the section 2-2 are given in Table 3. The reconstruction results corresponding to this numerical phantom study are encouraging as the hyperelastic parameters for the Veronda-Westmann model were reconstructed with high accuracy.

Table 3: The initial guess, true value of the parameters, calculated value of the parameters, number of iteration required to reach these values, the tolerances used as convergence criteria and the error percentage of the calculated values.

Veronda Westmann	Initial Guess	True Value	Calculated Value	Iteration Number	Tolerance (tol %)	Error (%)
C1	0.01	0.0014	0.00139	15	0.1	0.71
C2	0.01	-0.0048	-0.00479	15	0.1	0.21
C3	20	5.0194	5.02	15	0.1	0.012

Fig. 7 shows the actual value for each parameter versus its reconstructed value in every iteration for the Veronda-Westmann model. These figures show that the proposed technique converges to accurate values rapidly for all parameters.

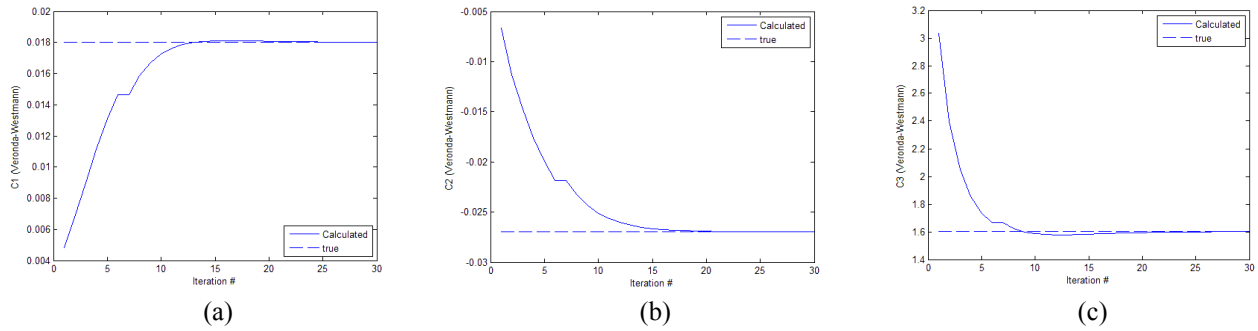


Fig. 7: a, b, c) The convergence of C1, C2, and C3 in the Veronda-Westmann form in the numerical phantom, respectively.

The stress-strain relationship corresponding to the true parameter values and the reconstructed parameter values are shown in Fig. 8.

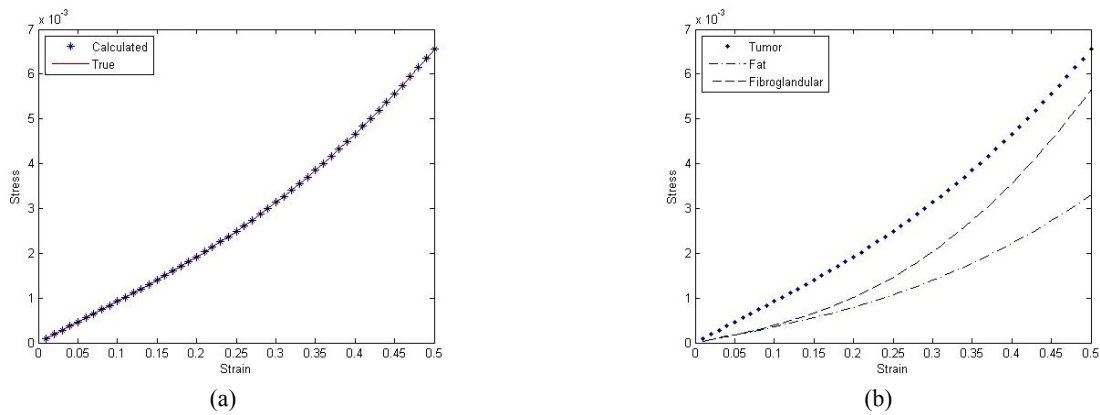


Fig. 8. a) true and reconstructed stress-strain curves of the tumor tissue of the Veronda-Westmann form, b) true stress-strain relationship of the outer tissue, middle tissue and tumor tissue for the Veronda-Westmann form in the numerical phantom.

### 3.2 Experimental Validation

Presence of an abnormality in the breast tissue and diagnosing its type can be done by comparing the mechanical behavior of the suspicious growth with the mechanical behavior of the normal breast tissues. Thus, to provide an efficient tool for breast cancer detection, the system must be capable of measuring relative parameters characterizing the tissues' mechanical behavior. Therefore, in the experimental study, we assume that the mechanical properties of the normal tissues as well as the tumor tissue are unknown. The iterative reconstruction approach is employed to reconstruct the hyperelastic parameters for all three tissue types in the phantom. Since our method only uses the displacement data of the phantom and no force information is used in the inverse problem, reconstructing the absolute values of the parameters is not possible. For absolute parameters reconstruction, the method requires that the hyperelastic parameters of at least one reference tissue is known.

Due to the lack of such a reference tissue in real applications, the method can reconstruct the relative values of the hyperelastic parameters. In fact this is the goal of this research, which may be sufficient for tumor detection and classification. Fig. 9 and Fig. 10 show the ratio of the parameters reconstructed for the inner cylindrical part (tumor) to the middle cubic part (fibrogland) and the outer cubic part (adipose) of the phantom corresponding to the Veronda-Westmann strain energy function, respectively.

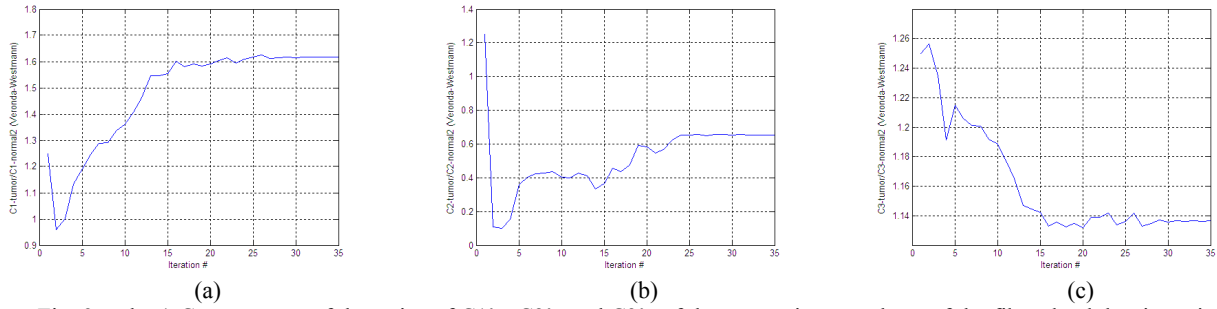


Fig. 9: a, b, c) Convergence of the ratios of C1's, C2's and C3's of the tumor tissue to those of the fibroglandular tissue in the Veronda-Westmann form, respectively.

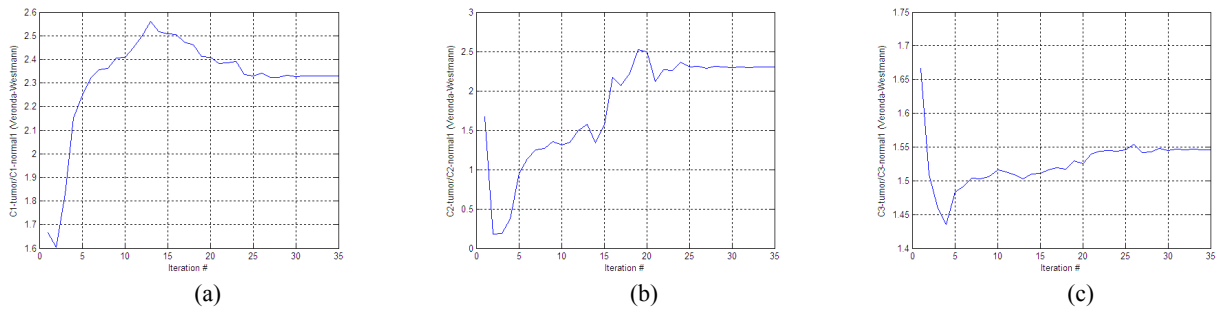


Fig. 10: a, b, c) Convergence of the ratios of C1's, C2's and C3's of the tumor tissue to those of the adipose tissue in the Veronda-Westmann form, respectively.

Fig. 11 shows the stress-strain curves corresponding to the reconstructed hyperelastic parameters versus the parameters calculated by applying the uniaxial compression test to the cylindrical sample of the tumor tissue type for the Veronda-Westmann model.

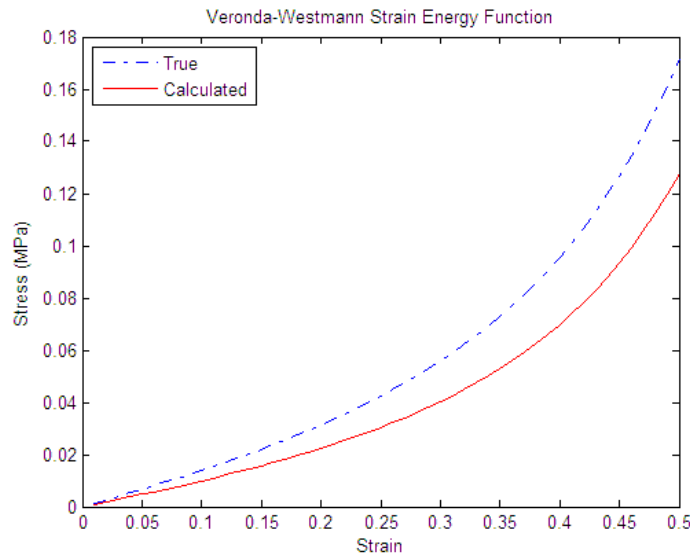


Fig. 11: True( resulted from uniaxial compression test) and reconstructed stress-strain curves of the tumor tissue for the Veronda-Westmann hyperelastic model

Tables 4 and 5 present the ratio of the C1's, C2's and C3's of the tumor tissue to the fibroglandular tissue and to the adipose tissue, for both reconstruction and uniaxial test results and their error percentage for the Veronda-Westmann model, respectively.

Table 4: Ratio of the C1's, C2's and C3's of the tumor tissue to the fibroglandular tissue, for both reconstruction and uniaxial test results and their error for the Veronda-Westmann model

	$C_{1_t}/C_{1_{n2}}$ (VW)	$C_{2_t}/C_{2_{n2}}$ (VW)	$C_{3_t}/C_{3_{n2}}$ (VW)
<b>Reconstructed</b>	1.616	0.654	1.136
<b>Uniaxial test</b>	1.378	0.566	1.291
<b>Error (%)</b>	17.243	15.518	12.001

Table 5: Ratio of the C1's, C2's and C3's of the tumor tissue to the adipose tissue, for both reconstruction and uniaxial test results and their error for Veronda-Westmann model.

	$C_{1_t}/C_{1_{n1}}$ (VW)	$C_{2_t}/C_{2_{n1}}$ (VW)	$C_{3_t}/C_{3_{n1}}$ (VW)
<b>Reconstructed</b>	2.329	2.299	1.546
<b>Uniaxial test</b>	2.116	2.833	1.662
<b>Error (%)</b>	10.065	18.845	6.999

#### 4. CONCLUSIONS AND DISCUSSIONS

Given the nonlinear nature of breast tissues, the reconstructed Young's modulus is valid only for a small range of strain. If the strain range becomes inconsistent as a result of applying a different pre-compression, the reconstructed Young's modulus will be totally different. Therefore, modeling the hyperelastic parameters of breast tissue is expected to address an important issue in elastography and make it more effective for cancer diagnosis. We believe that this approach has a good potential to lead to the development of a novel imaging technique for breast cancer assessment. This reconstruction technique can be also used to provide *in vivo* hyperelastic parameters of tissues that are critical to estimate soft tissues deformation undergoing large amounts of compression. Such estimation can pave the way for developing effective tools for interventional procedures planning. Furthermore, since this elastography approach takes into account both geometric and intrinsic nonlinearities, it can be used effectively in conjunction with elastography procedures where the tissue is significantly compressed to increase signal to noise ratio of displacement. The latter could lead to major improvement of elastography images.

In this work we presented further developments and validation of a novel nonlinear elastography technique [1]. In this technique, the hyperelastic parameters reconstruction was performed using the presented iterative approach. The problem is formulated as an inverse problem in which the parameters are updated at each iteration until convergence is achieved. Numerical analysis of our work in [1] was extended to incorporating the method with the Veronda-Westmann hyperelastic model. This model has exponential form and has gained a lot of interest in breast tissue modeling. The goal of this numerical validation was to measure the hyperelastic properties of the tumor tissue, assuming that the hyperelastic parameters of the normal tissues are known. The reconstruction showed encouraging results in constructing the hyperelastic properties of the tumor tissue. As reported in Table 3, all parameters were reconstructed with high accuracy. The results demonstrated that it is feasible to accurately reconstruct breast tissue hyperelastic parameters from measured displacement data. Convergence was achieved in a small number of iteration than the Yeoh and Polynomial models as reported in [1], and the error in reconstruction was less than 1%. This demonstrates the efficiency of the Veronda-Westmann model compared to the Yeoh and Polynomial models.

For experimental validation of the method, we constructed a tissue mimicking phantom using Polyvinyl Alcohol (PVA) that exhibits nonlinear mechanical behavior. We also used cylindrical samples of each tissue type to measure their hyperelastic properties independently using uniaxial tests. The results show that the relative reconstruction yields acceptable results. The reconstructed ratios were constructed with less than 20% error. The results also show that, although the parameters are reconstructed with about 20% error, the stress-strain curves of the actual parameters versus the reconstructed parameters are very close to each other. This is due to the fact that the cost function of our inverse problem is formulated in a way that it minimizes the difference between the experimental and calculated stress versus

strain relationship in a least squares manner. Therefore, the agreement between the experimental and calculated stress-strain curves was better than the parameters agreement. This agreement is even higher in the beginning of the curves where the tissue is still in the linear portion of its mechanical behavior. Another fundamental difference between the reconstructed parameters and the parameters obtained from uniaxial test is that the reconstructed parameters are obtained from fitting the measured displacements to a complex loading situation where all tensor stress components are present. This is not the case with a uniaxial test where only one stress component is present. This fundamental difference accounts for part of the disagreement. The accuracy achieved in this phantom study is reasonably good considering that there are inevitable several issues in the experiments. We speculate that this accuracy is adequate for the purpose of breast cancer detection and diagnosis.

## REFERENCES

- [1] Mehrabian H., Samani A., "An iterative hyperelastic parameters reconstruction for breast cancer assessment", Proc. SPIE, Vol. 6916, 69161C (2008).
- [2] Mehrabian H., Karimi H., Samani A., "Accurate optical flow field estimation using mechanical properties of soft tissues", Proc. SPIE, Vol. 7262 (2009).
- [3] World Health Organization International Agency for Research on Cancer (June 2003)., "World Cancer Report". Retrieved on 2008-02-03 (2008).
- [4] World Health Organization (February 2006)., "Fact sheet No. 297: Cancer". Retrieved on 2007-04-26, (2007)
- [5] Sinkus R., Weiss S., Wigger E., Lorenzen J., Dargatz M., Kuhl C., "Nonlinear elastic tissue properties of the breast measured by MR-elastography: initial in-vitro and in-vivo results" Proc. ISMRM 10th Annual Meeting 33, C (2002).
- [6] Gao L., Parker K. L., Lerner R. M., and Levinson S. F., "Imaging of the elastic properties of tissue-A review". Ultrasound in Med. & Biol., Vol. 22, No. 8, pp. 959-977 (1996).
- [7] Varghese T., Ophir J., Krouskop T. A., "Non-linear stress-strain relationships in tissue and their effect on the contrast-to-noise ratio in elastograms". Ultrasound in Med. & Biol., Vol. 26, No. 5, pp. 839-851 (2000).
- [8] Samani A., Bishop J., Plewes D. B., "A constrained modulus reconstruction technique for breast cancer assessment", Medical Imaging, IEEE Transactions on Medical Imaging, vol. 20, pp. 877-885 (2001)
- [9] Gokhale N. H., Barbone P. E., Oberai A. A., "Solution of the nonlinear elasticity imaging inverse problem: The compressible case," Inverse Problems, vol. 24, (2008).
- [10] Samani A., Plewes D. B., "A method to measure the hyperelastic parameters of ex vivo breast tissue samples," Physics in Medicine and Biology, vol. 49, pp. 4395-4405 (2004).
- [11] Watler P. K., Cholakis C. H., Sefton M. V., "Water content and compression modulus of some heparin-PVA hydrogels." Biomaterials 9: 150-154 (1988).
- [12] Ratner B. D., "Biomedical applications of synthetic polymers". In: Allen G, Bevington JC, editors. Comprehensive Polymer Science: The Synthesis, Characterization, Reactions and Applications of Polymers", Vol 7. Toronto: Pergamon Press. p 201-247 (1989).
- [13] Watase M., Nishinari K., Nambu M., "Rheological properties of an anomalous poly(vinyl alcohol) gel". Polym Commun 24:52-54 (1983).
- [14] Nagura M., Hamano T., Ishikawa H., "Structure of poly(vinyl alcohol) hydrogel prepared by repeated freezing and melting". Polymer 30: 762-765 (1989).
- [15] Peppas N. A., Stauffer S.R., "Reinforced uncrosslinked poly(vinyl alcohol) gels produced by cyclic freezing-thawing process: A short review". J Control Release 16:302-310 (1991).
- [16] Samani A., Bishop J., Luginbuhl C., Plewes D. B., "Measuring the elastic modulus of ex vivo small tissue samples" Physics in Medicine and Biology, vol. 48(14): pp. 2183-2198 (2003).
- [17] Horn B. K. P., Schunck B. G., "Determining optical flow", Artificial Intelligence 17: 185-204, (1981).